Influence of Oxygen Substoichiometry on the Dielectric Properties of $BaTiO_{3-\delta}$ Nanoceramics Obtained by Spark Plasma Sintering

Christophe Voisin, Sophie Guillemet-Fritsch,* Pascal Dufour, and Christophe Tenailleau

Institut Carnot CIRIMAT, UMR CNRS-UPS-INP 5085, Université de Toulouse, 118 route de Narbonne, 31062, Toulouse Cedex 9, France

Hyuksu Han and Juan C. Nino

Department of Materials Science and Engineering, University of Florida, Gainesville, Florida 32611

Oxygen-deficient $BaTiO_{3-\delta}$ nanoceramics were prepared by spark plasma sintering. Partially reduced raw nanopowders led to unusual dielectric properties. A short postsintering treatment was performed to reach a high $\varepsilon_r/\tan\delta$, which makes them attractive for industrial applications such as low-frequency capacitors. Surprisingly, our ceramics also remained black even after annealing for 5 days at 850°C in air, indicating the presence of barriers against oxygen diffusion. This exceptional behavior in pure barium titanate was consistent with a core–shell structure made of semiconductive grains and insulating grain boundaries, due to the presence of Ti^{3+}/Ti^{4+} and oxygen vacancies.

Introduction

Because of its interesting electrical properties, barium titanate, $BaTiO_3$, has become one of the most successful dielectric materials for electronic applications such as thermistors, multilayer ceramic capacitors (MLCCs), and pressure sensors.[1–3] Many studies have been carried out recently on the sintering of pure [4–6] or doped $BaTiO_3$ ceramics[7,8] by the spark plasma sintering (SPS) technique. The SPS technique offers the possibility to obtain ceramics with small grain size given the relatively low temperature and short time

*guillem@chimie.ups-tlse.fr

DOI:10.1111/ijac.12058

when compared with conventional sintering techniques. As shown in our previous work,[9] $BaTiO_3$ ceramics, when sintered by SPS, exhibit unusual electrical properties with colossal relative permittivity in the range of several hundred thousands at room temperature and kHz frequencies.

The SPS process takes place under vacuum atmosphere, and the nanosized powder is introduced into a graphite die. Consequently, resulting nanosized-grain ceramics $BaTiO_{3-\delta}$ are oxygen deficient, which is visually evidenced by the dark blue color of the pellets. It is now well established that the oxygen substoichiometry is the result of a high concentration of oxygen vacancies.[10] At the same time, Ti^{4+} is reduced to Ti^{3+} as a charge compensation mechanism.[11] Given this, a postsintering annealing treatment is customarily required to reoxidize ceramics. Then, the samples usually regain the original white (cream) color of the starting powder. Despite this well-known methodology for conventional $BaTiO_3$ processing, there are no extensive studies on the effect of the annealing parameters on samples sintered by SPS. To date, most of the thermal treatments reported in literature consist of heating runs under an oxidizing atmosphere for a given time, usually up to 12 h.[12,13] Conversely, many reports have been made on the oxygen diffusion during the reoxidation process of base metal electrode MLCCs obtained after conventional sintering under a reducing atmosphere.[14,15] For example, Yang *et al.* [16,17] revealed that in $BaTiO_3$-Ni MLCCs, $BaTiO_3$ becomes an n-type semiconductor due to the oxygen vacancies created during the co-firing process. Furthermore, depletion charge layers are formed at grain boundaries,[18] and these layers act as double Schottky barriers against the mobility of oxygen vacancies. In addition, Takashi Oyama *et al.* [19] showed that the grain boundaries will also limit the diffusion of oxygen vacancies, particularly in small-grain-size ceramics, thereby making them more difficult to reoxidize. However, this barrier to reoxidation in nanoceramics has not been investigated or reported during the annealing of SPS $BaTiO_3$ ceramics.

In this work, the reoxidation process of pure $BaTiO_3$ nanoceramics obtained by SPS was studied. The influence of various parameters of the heat treatment (temperature, dwell time, cooling rate) on the dielectric properties of the material was investigated. It has been shown before that for $BaTiO_3$ ceramics prepared by conventional sintering,[20] a change in Ba/Ti ratio affects the sintering behavior and the microstructure, which also influences the final dielectric properties of the ceramics. Therefore, ceramics containing varying Ba/Ti ratios were also studied to understand better the latter properties. Finally, a mechanism to explain the unusual electrical properties of SPS nanograin $BaTiO_3$ ceramics is here proposed.

Experimental Procedure

Powder Synthesis

The $BaTiO_3$ nanopowders were synthesized by an oxalate precipitation route. The procedure was described in detail in a previous paper.[9] $BaCl_2{\cdot}2H_2O$ (Prolabo) and $TiCl_3$ (Prolabo) were used as precursors for three batches (A1, A2, and A3), while $TiOCl_2$ (Prolabo) was used as Ti precursor for an additional batch (B). The precursors were weighted in appropriate proportions to control the powder stoichiometry, dissolved in water, and then added to an ethanolic oxalic acid solution. The A1, A2, and A3 batches have, respectively, a Ba/Ti ratio equal to 0.9, 0.95, and 1. The B powder has a Ba/Ti ratio of 1. The solution was stirred and aged for 5 h, then centrifuged, and dried overnight at 80°C. The oxide powders were obtained after calcination at 850°C for 4 h in static air. In addition, a commercial $BaTiO_3$ powder (Ba/Ti=1) from PI-KEM (Grade HPB-1000, average grain size of 50 nm) was studied for comparison.

Spark Plasma Sintering (SPS)

To densify the $BaTiO_3$ nanopowders, SPS was carried out using a Dr. Sinter 2080 device from Sumitomo Coal Mining (Fuji Electronic Industrial, Saitama, Japan). The same processing parameters were used for all the compositions. Briefly, 0.9 g of each batch was loaded in an 8-mm-inner-diameter graphite die. A sheet of graphitic paper was placed between the punch and the powder as well as between the die and the powder for easy removal of the pellet after sintering. Powders were sintered in vacuum (residual cell pressure < 10 Pa). A pulse pattern of twelve current pulses followed by two periods of zero current was used. A heating rate of 25°C/min was used from 600 to 1150°C, where a 3-min dwell time at the sintering temperature was applied. An optical pyrometer focused on a small hole at the surface of the die was used to measure and monitor the temperature. A uniaxial pres-

sure of 50 MPa was applied 2 min before reaching the dwell temperature. After the 3-min dwell, the electric current was switched off and the pressure was released. *In situ* dilatometry-based shrinkage curves for the different powders were recorded during the sintering process. The as-sintered pellets presented a thin carbon layer due to graphite contamination from the graphite sheets. This layer was removed by polishing the surface. In a previous work,[21] the presence of residual carbon due to SPS processing technique was determined through the spectrometric quantification of CO_2 and appeared to be very low with a concentration of 93 ppm. Samples appeared dark blue, consistent with the presence of Ti^{3+} caused by the reducing atmosphere used during SPS (low vacuum) as previously demonstrated using X-ray photoelectron spectroscopy (XPS).[21] SPS pellets were annealed in oxidizing atmosphere in an attempt to restore the oxygen stoichiometry. Different parameters of the thermal treatment (temperature, time, cooling rate, and atmosphere) were analyzed.

Characterization

The chemical composition of the different oxide powders (Ba/Ti ratio) was determined using induced coupled plasma–atomic emission spectroscopy (ICP-AES) with a JY 2000 device (Horiba Jobin Yvon, Kyoto, Japan). The particle size and morphology of the powders were observed with a field emission gun scanning electron microscope (FEG-SEM, JSM 6700F, JEOL, Tokyo, Japan) and a high-resolution transmission electron microscope (HRTEM, JEM 2100F, JEOL). The crystalline structure was investigated by X-ray diffraction analysis using a D4 Endeavor X-ray diffractometer (CuK_α = 0.154056 nm and CuK_β=0.154044 nm; Bruker AXS, Karlsruhe, Germany) from 20° to 80° (2-theta). To identify the oxidation state of titanium cations, electron paramagnetic resonance (EPR) spectra were recorded at 300 K using a Bruker Elexsys E500 EPR spectrometer. The density of the pellets was determined by the Archimedes method using an ARJ 220-4M balance (KERN, Murnau-Westried, Germany). Prior to electrical measurements, the ceramic disks were coated with thin gold electrodes (thickness ~ 30 nm) by sputtering (108 Auto, Cressington Scientific Instruments, Watford, U.K.). The relative permittivity and the dielectric losses were obtained from impedance measurements using a 4294A Impedance Analyzer (Agilent Technologies, Palo Alto, CA) in the range of 100 Hz to 40 MHz at room temperature and an applied voltage of 1 V. For temperature dependence of the dielectric properties, the electroded samples were placed in a closed cycle cryonic workstation (CTI 22, Cryo Industries of America, Manchester, NH) and measurements were taken as a function of temperature (20 K ~ 300 K) using an Agilent 4284A LCR meter.

Results and Discussion

$BaTiO_3$ Powders

Phases and grain sizes of the synthesized powders and sintered ceramics are presented in Table I. The FEG-SEM images of the $BaTiO_3$ powders of different compositions prepared are shown in Fig. 1. Powders A1, A2, A3, and B present a morphology similar to small particles, mostly agglomerated (Fig. 1a–d). It can be seen that the A1 and A2 powders have a particle size of about 80 nm, while the A3 and B powders have a higher particle size of ~150 nm. It is important to note that the as-synthesized A1, A2, and A3 powders have a light yellow color that can be attributed to the presence of Ti^{3+} cations, whereas the B powder is white. The presence of Ti^{3+} was confirmed by the EPR spectra as shown in Fig. 2. At 3400 Gauss, the representative signal of Ti^{3+} [22] is observed for each composition (A1 to A3), while a very low signal is observed for the B powder. No signal is observed for the reference powder from PI-KEM. Furthermore, it is also clear that the calcination treatment performed at 850°C for 4 h was not enough to fully oxidize the Ti^{3+} cations of the A1, A2, and A3 powders.

X-ray diffraction patterns corresponding to the powders are presented in Fig. 3. As expected, all powders crystallize in the cubic perovskite structure due to the small particle size.[23,24] For the powders A1 and A2, an additional phase, $BaTi_2O_5$, is also observed. It is not surprising as there is a titanium-excess in those powders. The amount of the $BaTi_2O_5$ phase, estimated from the relative peak intensities, increases from 1 wt% to 5 wt% as the Ba/Ti ratio decreases from 0.95 to 0.90. For the powders A3 and B with Ba/Ti = 1, no secondary phase is formed. These observations are in agreement with the phase diagram reported by Lee *et al.*[25]

$BaTiO_{3-\delta}$ Ceramics

The sintered materials obtained by SPS displayed a dark blue color due to the reducing sintering

Table I. Characteristics of the Synthesized Powders and the Corresponding Ceramics Sintered by Spark Plasma Sintering (SPS) at 1150°C (compositions Ba/Ti = 0.9, 0.95, and 1)

		Powder		Ceramic		
Powder	Composition (Ba/Ti ratio)	Phases	Particle size	Phases	Grain size	Densification (%)
A1	0.9	C $BaTiO_3$ + $BaTi_2O_5$	80 nm	C + T $BaTiO_3$ + $Ba_4Ti_{12}O_{27}$	150 nm	98
A2	0.95	C $BaTiO_3$ + $BaTi_2O_5$	80 nm	C + T $BaTiO_3$ + $Ba_4Ti_{12}O_{27}$	150 nm	98
A3	1	C $BaTiO_3$	150 nm	C + T $BaTiO_3$	200 nm	98
B	1	C $BaTiO_3$	150 nm	C + T $BaTiO_3$	200 nm	98
Reference from PI-KEM	1	C $BaTiO_3$ + $BaCO_3$	50 nm	T $BaTiO_3$	5 μm	98

C, cubic perovskite; T, tetragonal perovskite.

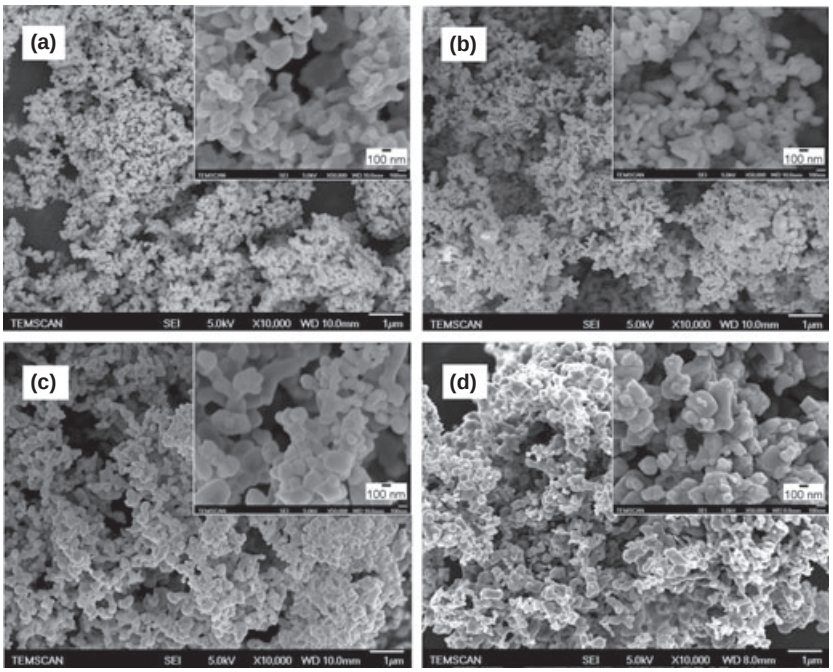

Fig. 1. FEG-SEM images of the $BaTiO_3$ powders: (a) A1 (Ba/Ti = 0.90); (b) A2 (Ba/Ti = 0.95); (c) A3 (Ba/Ti = 1); and (d) B (Ba/Ti = 1).

atmosphere.[9,26] Ti-excess $BaTiO_{3-\delta}$ ceramics (A1 and A2) and the $BaTiO_{3-\delta}$ ceramics with Ba/Ti = 1 (A3 and B) present a high densification of 98%.

The freshly fractured ceramics were observed by FEG-SEM (Fig. 4). The grain size is about 150 nm for A1 and A2 (Fig. 4a,b) and 200 nm for A3 and B

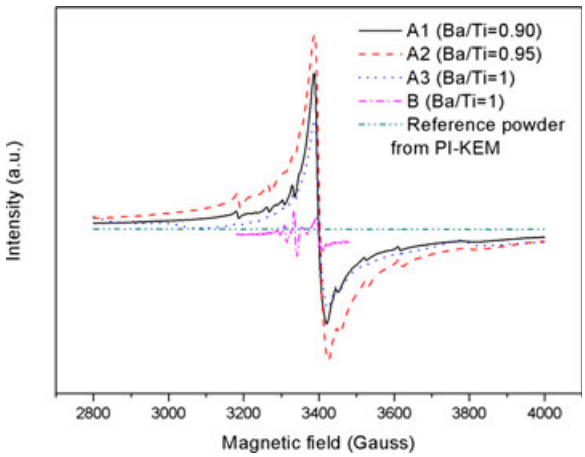

Fig. 2. Electron paramagnetic resonance(EPR) spectra of the $BaTiO_3$ powders with different Ba/Ti ratios.

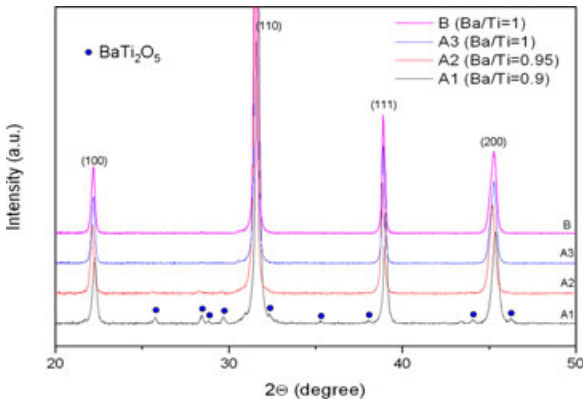

Fig. 3. X-ray diffraction patterns of the $BaTiO_3$ powders.

(Fig. 4c–d). Samples of A2 and A3 ceramics were observed by HRTEM (Fig. 5a). A dense and homogenous grain structure is evidenced. Ceramics contain compact and well-crystallized nanograins, and grain boundaries are very small with a width in the nanometer scale.

Figure. 6 shows the X-ray diffraction patterns of the $BaTiO_{3-\delta}$ ceramics. The A1, A2, A3, and B ceramics consist of a mixture of cubic and tetragonal perovskite phases, as shown by the broadening of the (200) peak (see insert Fig. 6). This is in agreement with previous results evidencing the coexistence of both phases after SPS sintering.[27] For the $BaTiO_{3-\delta}$ ceramics A3 and B with Ba/Ti = 1, no secondary phase is formed. On the contrary, $Ba_4Ti_{12}O_{27}$ (1–5 wt%) is observed as a secondary phase for the Ti-rich $BaTiO_{3-\delta}$ ceramics (A1 and A2). These results are in agreement with those of Lee *et al.*[28] who showed that the $Ba_4Ti_{12}O_{27}$ phase is found when annealing Ti-rich $BaTiO_3$ powder under low PO_2 conditions. The reduction of some Ti^{4+} to Ti^{3+} explains the formation of this additional phase, considering that the composition can be written as $Ba_4Ti_2^{3+}Ti_{10}^{4+}O_{27}$. The amount of this phase increases from 1 wt% to 5 wt%, as the Ba/Ti ratio decreases.

Dielectric Characteristics

After SPS treatment, the as-sintered ceramics (A1, A2, A3, and B) present colossal relative permittivity of $\sim 2.5*10^6$ regardless of compositions and synthesis history. By comparison, the ceramics prepared from the commercial powder (PI-KEM) under the same sintering conditions show an order of magnitude lower relative permittivity. It is important to note that these measured values are associated with high dielectric losses and therefore are not representative of a capacitive behavior and, therefore, are not relevant for industrial applications. It is then necessary to anneal the ceramics to decrease the dielectric loss and regain their insulating behavior. The annealing parameters studied here were the cooling rate and the dwell time.

The initial annealing parameters were taken from one of our previous studies and can be summarized as follows: anneal at 850°C during 2 h in air with a heating and a cooling rate of 150°C/h.[21] After the annealing process, the A1, A2, and A3 ceramics remain dark blue, while the B ceramic becomes white.

In this work, a thorough study of the influence of different annealing parameters was performed on A3 (Ba/Ti = 1) ceramics, and the results are presented in the following subsection. The optimum parameters were then used for the reoxidation of the composition A2 (Ba/Ti = 0.95), which shows the most interesting properties.

$BaTiO_{3-\delta}$ Ceramics with Ba/Ti = 1 (A3)

Influence of the Cooling Rate—The influence of the cooling rate on the dielectric properties after the annealing process performed in air on a set of $BaTiO_{3-\delta}$ ceramics with Ba/Ti = 1 is shown in Fig. 7. The dielectric properties are listed in Table II. Two ceramics were introduced into the hot furnace held at

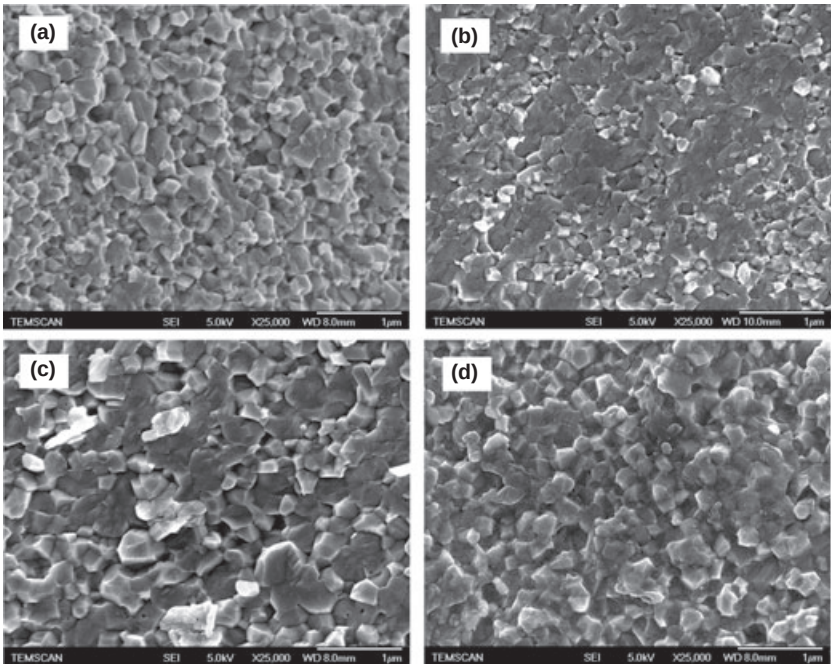

Fig. 4. FEG-SEM images of the $BaTiO_3$ ceramics: (a) A1 (Ba/Ti = 0.90); (b) A2 (Ba/Ti = 0.95); (c) A3 (Ba/Ti = 1); and (d) B (Ba/Ti = 1).

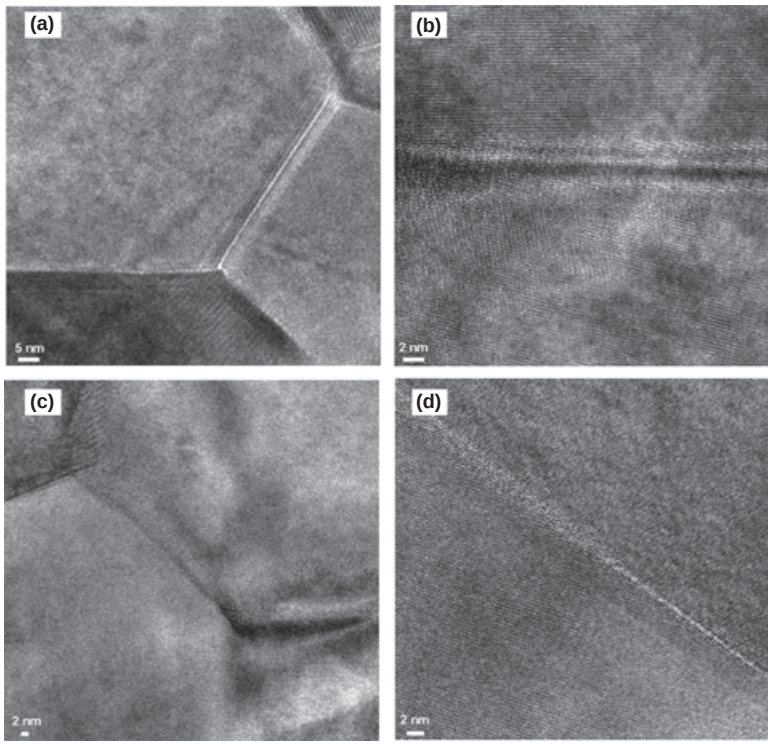

Fig. 5. HRTEM images of the $BaTiO_3$ ceramics: (a, b) A2 (Ba/Ti = 0.95); and (c, d) A3 (Ba/Ti = 1).

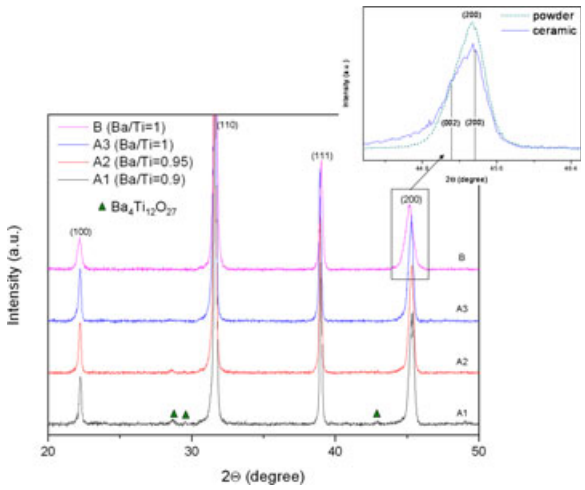

Fig. 6. X-ray diffraction patterns of the $BaTiO_3$ ceramics.

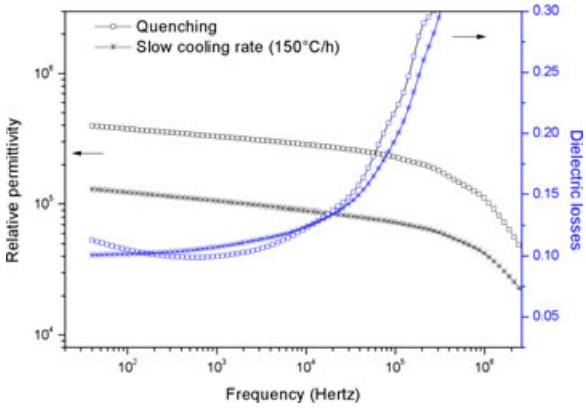

Fig. 7. Influence of the cooling rate during the annealing process at 850° C during 5 min in air of A3 (Ba/Ti = 1) on the dielectric permittivity and dielectric loss.

850°C, during the dwell, and maintained in this temperature for only 5 min. Then, one ceramic was quenched in air, while the other was cooled down with a low cooling rate (150°C/h). A higher relative permittivity is obtained for the quenched ceramic ($\varepsilon_r = 3.2 \times 10^5$), up to three times the value of the ceramic cooled down slowly ($\varepsilon_r = 1.1 \times 10^5$). However, the ceramics present very similar and still high dielectric losses ($\tan\delta = 0.10$ and 0.11 for the quenched and slow-cooled samples, respectively, at room temperature and 1 kHz). So, quenched samples showed higher relative permittivities than slow-cooled samples. The slow cooling process allows more Ti^{3+} to be oxidized in Ti^{4+}, and the number of charge carriers therefore decreases. The relative permittivity decreases consequently. In the meantime, the grain boundaries (GBs) become quickly saturated by the oxygen vacancies upon cooling and the dielectric loss reaches rapidly a small value. No further variation of the dielectric loss is observed as the "frozen" states of the oxygen vacancies in GB act as resistive interfaces. This will be discussed later.

Influence of the Reoxidation Time—To study the influence of the reoxidation time on the dielectric properties, the ceramic was annealed in air at 850°C for 5 min and then quenched. After the electrical measurements, the sample was introduced again in the furnace under the same conditions once the thin layer of gold was removed. The process was repeated several times until reaching a reoxidation time of 45 min. The thin layer of gold was removed by polishing, and the absence of gold at the surface of the ceramic was checked by X-ray diffraction. The relative permittivity and the loss of $BaTiO_{3-\delta}$ ceramics at selected frequencies in air are listed in Table III as a function of the annealing time at 850°C. The relative permittivity

Table II. Dielectric Properties of the A3 Ceramic (Ba/Ti = 1) Annealed in Air at 850°C During 5 min and Slowly Cooled (~150°C/h) or Quenched

	Frequency					
	10^2 Hz		10^3 Hz		10^4 Hz	
Cooling rate	ε	tanδ	ε	tanδ	ε	tanδ
Slow (~150°C/h)	122,322	0.10	105,975	0.11	88,787	0.12
Fast (quenching)	375,376	0.10	318,309	0.10	283,665	0.12

Table III. Dielectric Properties of the A3 Ceramic (Ba/Ti=1) Annealed for Different Time at 850°C in Air Followed by Quenching

Annealing time (min)	Frequency					
	10^2 Hz		10^3 Hz		10^4 Hz	
	ε	tanδ	ε	tanδ	ε	tanδ
5	400,895	0.10	340,724	0.10	283,884	0.12
10	370,496	0.13.	324,066	0.12	280,149	0.15
15	329,147	0.12	279,322	0.12	232,257	0.15
30	171,166	0.11	145,971	0.12	120,386	0.15
45	121,148	0.11	103,408	0.11	85,697	0.15

Table IV. Dielectric Properties of the A2 Ceramic (Ba/Ti=0.95) Annealed for Different Times at 850°C in Air Followed by Quenching

Annealing time (min)	Frequency					
	10^2 Hz		10^3 Hz		10^4 Hz	
	ε	tanδ	ε	tanδ	ε	tanδ
5	1,046,380	0.11	942,444	0.09	864,943	0.10
10	836,005	0.11	744,584	0.09	674,387	0.12
15	487,419	0.06	458,842	0.05	433,470	0.08
30	288,911	0.05	270,889	0.05	252,758	0.08

decreases when increasing the annealing time. It varies from $\varepsilon_r = 3.4 \times 10^5$ for a reoxidation time of 5 min to 1.0×10^5 for a time of 45 min. On the contrary, the dielectric losses of the material are not influenced by the annealing time as the value of tanδ remains close to 0.12.

$BaTiO_{3-\delta}$ Ceramics with Ba/Ti = 0.95 (A2)—After annealing using the optimum parameters for sample A3 (i.e., 850°C, 5 min in air, and air-quenched), sets of $BaTiO_{3-\delta}$ ceramics with a Ba/Ti ratio of 0.95 showed the highest permittivity-to-loss ratio. Therefore, the annealing time was re-optimized for those ceramics as well. The values of the relative permittivity and the dielectric losses (at 1 kHz) of ceramic A2 for different annealing times are listed in Table IV. The relative permittivity decreases when increasing the annealing time as it was the case for the ceramics with Ba/Ti = 1. The relative permittivity varies from $\varepsilon_r = 9.4 \times 10^5$ for a reoxidation time of 5 min to $\varepsilon_r = 2.7 \times 10^5$ for 30 min. The dielectric losses also decrease when increasing the annealing time of the ceramic up to 15 min. For annealing times higher than 15 min, the values of the dielectric losses remain stable at values below 0.05. Therefore, a 15-min annealing time was determined to be the optimum for obtaining a ceramic presenting the most promising properties: a high relative permittivity and low dielectric losses. When processed in this particular way, A2 $BaTiO_{3-\delta}$ ceramics present very attractive properties: $\varepsilon_r = 4.6 \times 10^5$ and tanδ = 0.05. This is presented in Fig. 8, where the frequency dependence of the relative permittivity and the dielectric loss of the ceramics with Ba/Ti = 1 and 0.95 are contrasted. The thermal treatment of the ceramics was identical (i.e., annealed in air at 850°C for 15 min and air-quenched). The dielectric permittivity of the A2 (Ba/Ti = 0.95) $BaTiO_{3-\delta}$ ceramic is about double that of A3 (Ba/Ti = 1) $BaTiO_{3-\delta}$ ceramic.

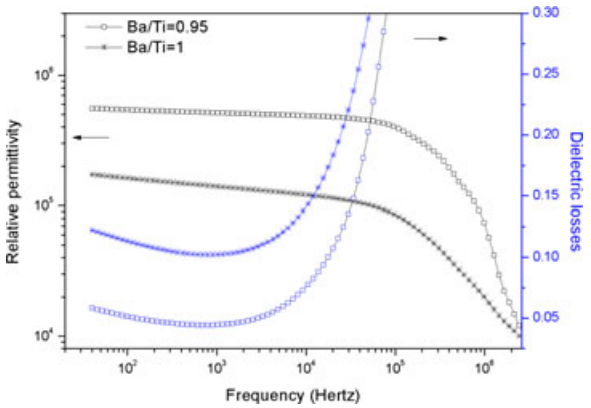

Fig. 8. Influence of the Ba/Ti ratio of a ceramic annealed at 850°C in air during 30 min followed by quenching on the dielectric permittivity and dielectric loss.

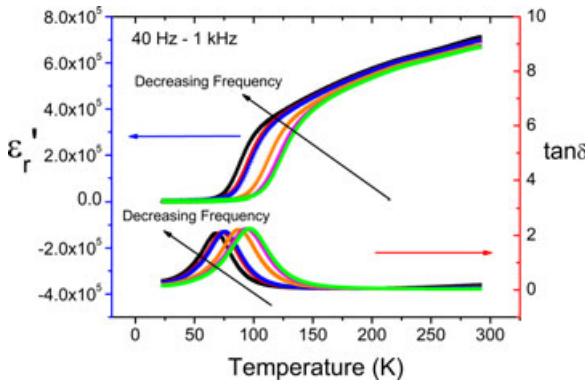

Fig. 9. Dielectric permittivity and dielectric loss of the ceramic A2 (Ba/Ti = 0.95) annealed at 850°C in air during 30 min followed by quenching, as a function of temperature.

Perhaps more interesting is the fact that the present work indicates that ceramics obtained after SPS sintering (which are in a reduced state) do not fully reoxidize after typical annealing treatments, but do recover dielectric characteristics. A mechanism explaining this interesting behavior is proposed in the following of this article. Between all ceramic compositions we studied, the best $\varepsilon_r/\tan\delta$ ratio was obtained for Ba/Ti = 0.95 (A2). The Ti-excess in the initial powder contributes to an increase in Ti^{3+} concentration associated with oxygen vacancies. When Ba/Ti $\leq$ 0.95, the secondary phase, $Ba_4Ti_2^{3+}Ti_{10}^{4+}O_{27}$, is observed by X-ray diffraction and could increase, at low extent, the amount of the reduced titanium ion in ceramics. But, as Ba/Ti decreases further, this secondary phase increases in the materials and the $\varepsilon_r/\tan\delta$ ratio is deteriorated. On the other hand, when Ba/Ti varies from 0.95 to 1, the secondary phase, if present, could not be seen by X-ray diffraction (XRD) and $\varepsilon_r/\tan\delta$ diminishes.

Artemenko *et al.*[29] investigated the reoxidation of $BaTiO_3$ at SiO_2 core–shell ceramics obtained by SPS and showed that the silica shell prevents the reoxidation. The oxygen-deficiency-related defects created during SPS sintering are blocked at the compositional interface with a semiconducting BT core. In our study, the $BaTiO_3$ material has no additional phase (apart from a small amount of $Ba_4Ti_{12}O_{27}$ observed in some cases only). However, in both cases, as oxygen vacancies are expected to be the dominant point defects, the observed resistance to reoxidation is related to the stability of these oxygen vacancies at the interfaces. Grain boundaries act as blocking barriers against oxygen diffusion.

Dielectric constant and dielectric losses of the A2 sample were also measured as a function of temperature (25 K ~ 300 K) across several frequencies in the space-charge region (40 Hz ~ 1 kHz). Fig. 9 shows that as the temperature decreases, the colossal permittivity of the A2 sample decreases in a step-like fashion, and dielectric loss peaks appeared, with the temperature of the occurrence of both features decreasing with decreasing frequency. This implies that the mechanism giving rise to colossal permittivity is a thermally activated process, consistent with space-charge dielectric relaxation. It is clear that the colossal permittivity up to the value of magnitude 10^5 is still maintained above 180 K and that the drop-off in the permittivity is completed by 50 K. This behavior is also observed in the well-known high-permittivity material $CaCu_3Ti_4O_{12}$ (CCTO).[30] To further investigate this phenomenon, a Debye relaxation model was applied where the relaxation frequency can be represented by the following expression:

$$\nu = \nu_o \exp\left(-\frac{E_A}{k_B T}\right)$$

where k_B, ν_o, and E_A represent the Boltzmann constant, the pre-exponential factor, and the activation energy required for relaxation, respectively. A maximum in the imaginary part of permittivity (ε_r'') arises when $\nu\tau = 1$ is satisfied, where τ is the dielectric relaxation time. Thus, the ε_r'' values were calculated from the permittivity and the dielectric losses, and the relaxation temperatures at the different frequencies (40 Hz ~ 1 kHz) were

extracted from the different maxima. The Arrhenius plot using the obtained values in the above equation is shown in Fig. 10. A linear fit is evident with an activation energy of 0.054 eV and an attempt-jump frequency of 3.57×10^7 Hz. These results indicate a space-charge relaxation phenomenon following Debye's theory, which would be here directly related to the interfacial polarization effect by oxygen vacancies localized in the grain boundaries and polarons hopping within the grains. An illustration of the mechanism responsible for the oxygen vacancy distribution and rearrangement after reoxidation is given in the schematic representation in Fig. 11. The number of oxygen vacancies in the as-sintered ceramics elaborated by the SPS process is related to the Ba/Ti ratio of the initial powder and the titanium source used during powder processing. The number of oxygen vacancies increases when decreasing the Ba/Ti ratio and/or using Ti^{3+}-containing raw powders ($TiCl_3$) instead of Ti^{4+} source ($TiOCl_2$). First, when annealing the ceramics in air at 850°C for a short time (15 min), the oxygen vacancies get reorganized and move toward the GB. In a

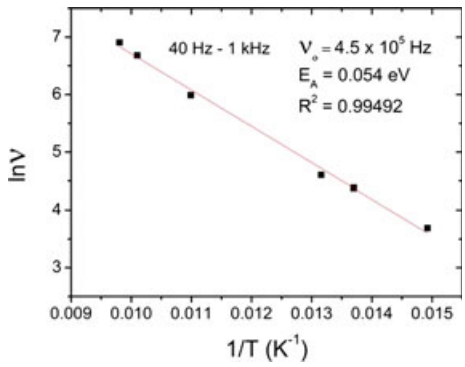

Fig. 10. Arrhenius behavior of relaxation extracted from dielectric measurements.

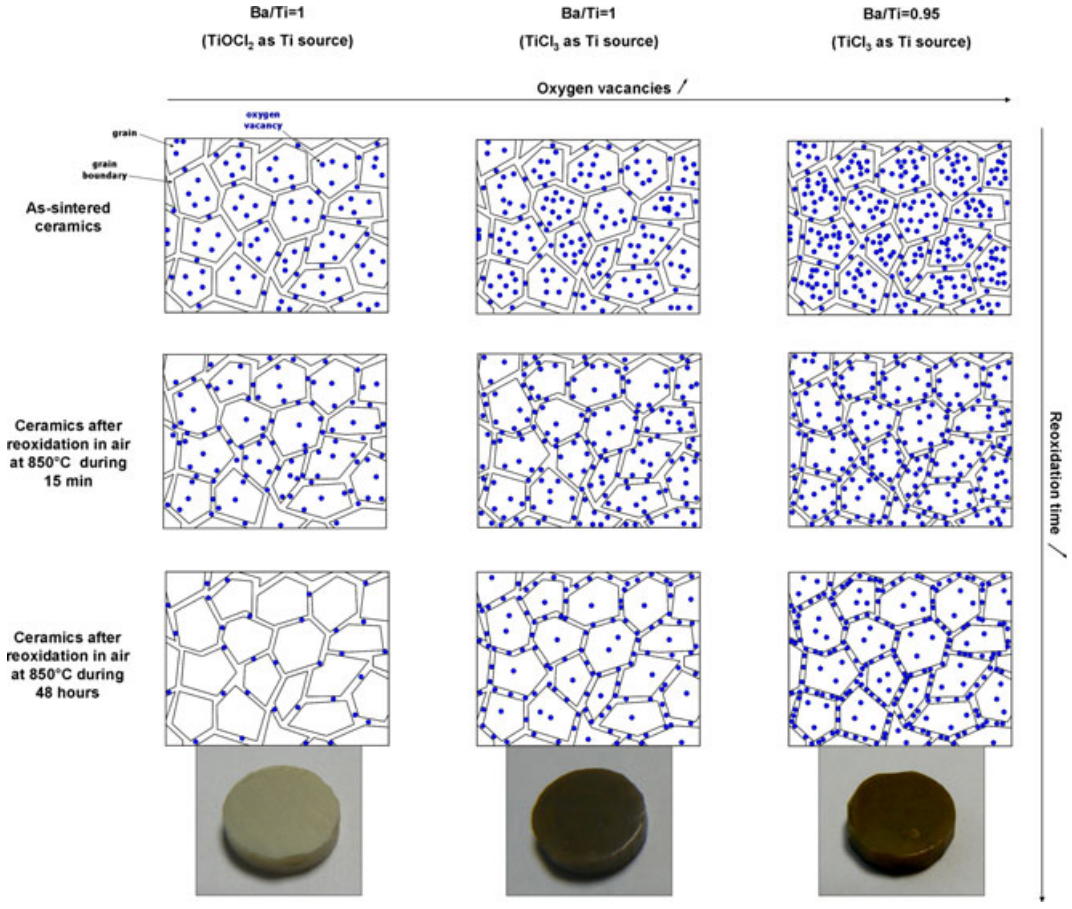

Fig. 11. Influence of the reoxidation time on the oxygen vacancies behavior in the ceramics of different compositions.

second time, after a long reoxidation time (48 h), in the case of ceramics elaborated with a Ti^{4+} source, most of the oxygen vacancies have been removed. The ceramic is totally reoxidized and of white color. Finally, for ceramics elaborated with a Ti^{3+} source, the numerous oxygen vacancies are quickly concentrated at the GB, which act as blocking barriers against any further oxygen diffusion, with a few of them that might remain in the grain cores. The ceramics could not be fully reoxidized and remain dark in color, even after 5 days of reoxidation time. A broadband dielectric spectroscopy study is currently being undertaken to evidence clearly the origin of colossal permittivity in our ceramics.

Conclusion

Nanometric powders of barium titanate with different Ba/Ti ratios were obtained by a coprecipitation synthesis followed by a thermal treatment in air using two different titanium sources. The powders synthesized from Ti^{3+} source ($TiCl_3$) and with a titanium-excess (Ba/Ti = 0.95) originally contain a large number of oxygen vacancies. After the spark plasma sintering process, the nanoceramics present a densification of 98% and are highly oxygen deficient. The as-sintered ceramics are conductive. Therefore, annealing is necessary to recover the insulating characteristics. Oxygen vacancies associated with Ti^{3+} cations contained in the powders and ceramics and their localization at grain boundaries seem to be the key factor to control the dielectric properties. The highest value of relative permittivity ($\varepsilon_r = 5 \times 10^5$) (at 1 kHz and room temperature) and the lowest dielectric losses ($\tan\delta = 5\%$) are obtained for a $BaTiO_{3-\delta}$ ceramics, with Ba/Ti = 0.95, annealed in air at 850°C for 15 min followed by air quenching. The obtained dense nanoceramics represent a very interesting engineered material for low-frequency capacitive applications.

Acknowledgment

The authors thank the DGAC for financial support (ISS2 project).

References

1. L. B. Kong, S. Li, T. S. Zhang, J. W. Zhai, F. Y. C. Boey, and J. Mad, "Electrically Tunable Dielectric Materials and Strategies to Improve their Performances," *Prog. Mater Sci.*, 55 [8] 840–893 (2010).
2. D. H. Yoon and B. I. Lee, "$BaTiO_3$ Properties and Powder Characteristics for Ceramic Capacitors," *J. Ceram. Process. Res.*, 3 [2] 41–47 (2002).
3. G. H. Haertling, "Ferroelectric Ceramics: History and Technology," *J. Am. Ceram. Soc.*, 82 [4] 797–818 (1999).
4. T. Takeuchi, E. B. Etourne, M. Tabuchi, and H. Kageyama, "Dielectric Properties of Spark-Plasma-Sintered $BaTiO_3$," *J. Mater. Sci.*, 34 [5] 917–924 (1999).
5. W. Luana, L. Gaob, H. Kawaokac, T. Sekinoc, and K. Niiharac, "Fabrication and Characteristics of Fine-Grained $BaTiO_3$ Ceramics by Spark Plasma Sintering," *Ceram. Int.*, 30 [3] 405–410 (2005).
6. B. Li, *et al.*, "Dielectric Properties of Fine-Grained $BaTiO_3$ Prepared by Spark-Plasma-Sintering," *Mater. Chem. Phys.*, 83 [1] 23–28 (2004).
7. N. El Horr, Z. Valdez-Nava, C. Tenailleau, and S. Guillemet-Fritsch, "Microstructure of $Ba_{1-x}La_xTiO_{3-\delta}$ Ceramics Sintered by Spark Plasma Sintering," *J. Eur. Ceram. Soc.*, 31 [6] 1087–1096 (2011).
8. A. Gheorghe, M. Cernea, R. Radu, and R. Trusca, "Application of Spark Plasma Sintering to Processing of Dense $Ba(Ti_{1-x}Sn_x)O_3$ (x = 0.13) Ceramic," *J. Alloy. Compd.*, 505 [1] 273–277 (2010).
9. Z. Valdez-Nava, S. Guillemet-Fritsch, C. Tenailleau, T. Lebey, B. Durand, and J. Y. Chane-Ching, "Colossal Dielectric Permittivity of $BaTiO_3$-Based Nanocrystalline Ceramics Sintered by Spark Plasma Sintering," *J. Electroceram.*, 22 238–244 (2009).
10. K. Watanabe, I. Sakaguchi, S. Hishita, N. Ohashi, and H. Haneda, "Visualization of Grain Boundary as Blocking Layer for Oxygen Tracer Diffusion and a Proposed Defect Model in Non Doped $BaTiO_3$ Ceramics," *Appl. Phys. Express*, 4 055801 3 (2011).
11. D. I. Woodward and I. M. Reaney, "Vacancy Ordering in Reduced Barium Titanate," *Appl. Phys. Lett.*, 84 [23] 4650–4652 (2004).
12. U. C. Chung, C. Elissalde, S. Mornet, M. Maglione, and C. Estournès, "Controlling Internal Barrier in Low Loss $BaTiO_3$ Supercapacitors," *Appl. Phys. Lett.*, 94 [7] 072903 3 (2009).
13. M. Hiroshi, "Electromechanical Properties of $BaTiO_3$ Ceramics Prepared by Spark Plasma Sintering and Other Methods," *Jpn. J. Appl. Phys.*, 48 [9] 09KD04 4 (2009).
14. M. R. Opitz, K. Albertsen, J. J. Beeson, D. F. Hennings, J. L. Routbort, and C. A. Randall, "Kinetic Process of Reoxidation of Base Metal Technology $BaTiO_3$-Based Multilayer Capacitors," *J. Am. Ceram. Soc.*, 86 [11] 1879–1884 (2003).
15. K. Kaneda, S. Lee, N. J. Donnelly, W. Qu, C. A. Randall, and Y. Mizuno, "Kinetics of Oxygen Diffusion into Multilayer Ceramic Capacitors During the Reoxidation Process and its Implications on Dielectric Properties," *J. Am. Ceram. Soc.*, 94 [11] 3934–3940 (2011).
16. G. Y. Yang, *et al.*, "Oxygen Nonstoichiometry and Dielectric Evolution of $BaTiO_3$. Part I—Improvement of Insulation Resistance with Reoxidation," *J. Appl. Phys.*, 96 [12] 7492–7499 (2004).
17. G. Y. Yang, *et al.*, "Oxygen Nonstoichiometry and Dielectric Evolution of $BaTiO_3$. Part II— Insulation Resistance Degradation under Applied Dc Bias," *J. Appl. Phys.*, 96 [12] 7500–7508 (2004).
18. R. Hagenbeck, "Electrical Properties of Grain Boundaries in Titanate Ceramics," *Solid State Phenom.*, 80–81 21–32 (2001).
19. T. Oyama, N. Wada, and H. Takagi, "Trapping of Oxygen Vacancy at Grain Boundary and its Correlation with Local Atomic Configuration and Resultant Excess Energy in Barium Titanate: A Systematic Computational Analysis," *Phys. Rev. B*, 82 [13] 134107 10 (2010).
20. J. K. Lee and K. S. Hong, "Roles of Ba/Ti Ratios in the Dielectric Properties of $BaTiO_3$ Ceramics," *J. Am. Ceram. Soc.*, 84 [9] 2001–2006 (2001).
21. S. Guillemet-Fritsch, Z. Valdez-Nava, C. Tenailleau, T. Lebey, B. Durand, and J. Y. Chane-Ching, "Colossal Permittivity in Ultrafine Grain Size $BaTiO_{3-x}$ and $Ba_{0.95}La_{0.05}TiO_{3-x}$ Materials," *Adv. Mater.*, 20 551–555 (2008).
22. T. Kolodiazhnyi and A. Petric, "Analysis of Point Defects in Polycrystalline $BaTiO_3$ by Electron Paramagnetic Resonance," *J. Phys. Chem. Solids*, 64 [6] 953–960 (2003).
23. M. T. Buscaglia, V. Buscaglia, M. Viviani, P. Nanni, and M. Hanuskova, "Influence of Foreign Ions on the Crystal Structure of $BaTiO_3$," *J. Eur. Ceram. Soc.*, 20 [12] 1997–2007 (2000).
24. X. H. Zhu, J. M. Zhu, S. H. Zhou, Z. G. Liu, N. B. Ming, and D. Hesse, "Microstructural Characterization of $BaTiO_3$ Ceramic Nanoparticles

Synthesized by the Hydrothermal Technique," *Solid State Phenom.*, 106 41 –46 (2005).
25. S. Lee and C. A. Randall, "Modified Phase Diagram for the Barium Oxide –Titanium Dioxide System for the Ferroelectric Barium Titanate," *J. Am. Ceram. Soc.*, 90 [8] 2589–2594 (2007).
26. Z. Valdez-Nava, *et al.*, "Structural Characterization of Dense Reduced $BaTiO_3$ and $Ba_{0.95}La_{0.05}TiO_3$ Nanoceramics Showing Colossal Dielectric Values," *J. Phys. Chem. Solids*, 72 [1] 17–23 (2011).
27. T. Takeuchi, M. Tabuchi, and H. Kageyama, "Preparation of Dense $BaTiO_3$ Ceramics with Submicrometer Grains by Spark Plasma Sintering," *J. Am. Ceram. Soc.*, 82 [4] 939–943 (1999).
28. S. Lee and C. A. Randall, "Comprehensive Linkage of Defect and Phase Equilibria Through Ferroelectric Transition Behavior in $BaTiO_3$-Based Dielectrics: Part 2. Defect Modeling Under Low Oxygen Partial Pressure Conditions," *J. Am. Ceram. Soc.*, 91 [6] 1753–1761 (2008).
29. A. Artemenko, *et al.*, "Linking Hopping Conductivity to Giant Dielectric Permittivity in Oxides," *Appl. Phys. Lett.*, 97 [13] 132901 3 (2010).
30. M. A. Subramanian, D. Li, N. Duan, B. A. Reisner, and A. W. Sleight, "High dielectric Constant in $ACu_3Ti_4O_{12}$ and $ACu_3Ti_3FeO_{12}$ Phases," *J. Sol. State Chem.*, 151 [2] 323–332 (2000).